IEEE Access
Multidisciplinary | Rapid Review | Open Access Journal

SPECIAL SECTION ON ADVANCED OPTICAL IMAGING FOR EXTREME ENVIRONMENTS

Received March 2, 2019, accepted March 12, 2019, date of publication April 1, 2019, date of current version April 15, 2019.

Digital Object Identifier 10.1109/ACCESS.2019.2908378

CT and MR Image Fusion Based on Adaptive Structure Decomposition

FAN ZHAO[1], GUIYING XU[2], AND WENDA ZHAO[2], (Member, IEEE)

[1]Dalian Institute of Chemical Physics, Chinese Academy of Sciences, Dalian 116023, China
[2]School of Information and Communication Engineering, Dalian University of Technology, Dalian 116024, China

Corresponding author: Wenda Zhao (zhaowenda@dlut.edu.cn)

This work was supported in part by the National Natural Science Foundation of China under Grant 61801077, Grant 61872056, and Grant 61771088, in part by the China Postdoctoral Science Foundation under Grant 2017M611221, and in part by the Fundamental Research Funds for the Central Universities under Grant DUT16RC(3)077.

ABSTRACT Computed tomography (CT) has an excellent performance in detecting dense structure, such as bones and implants, while magnetic resonance (MR) provides high-resolution information for soft issues. To obtain sufficient and accurate information for diagnosis, we propose a CT and MR image fusion method via adaptive structure decomposition to combine the complementary information. First, on the basis of different scales of issues, we adaptively decompose the source images into sub-bands (bands of small, middle, and large issues) by a spectral total variation method. Second, based on the interpretability of sub-bands, for the small scale and middle scale of issues, we extract the edge information from the sub-bands and design the fusion weight by the local edge energy. And for the large scale of issues, we design the fusion weight by the local intensity energy. Third, we reconstruct the fused image. The experimental results demonstrate the superiority of the proposed method on both subjective and objective assessments.

INDEX TERMS CT and MR image fusion, spectral TV, adaptive structure decomposition.

I. INTRODUCTION

Medical imaging has drawn multiple attention because it is performing a critical role in clinical applicability such as diagnosis of diseases and the planning of treatment. Due to the different mechanical principles of medical imaging instruments, the produced medical images focus on restricted parts of issues/organs. Therefore, the limited information is provided respectively. The computed tomography (CT) has an excellent performance on detecting dense structure such as bones and implants and, magnetic resonance (MR) provides high-resolution information for soft issues [1]–[4]. To obtain sufficient and accurate information, physicians have to analyze CT and MR images respectively, which leads to inconvenience. Under this circumstance, CT and MR image fusion provides an easier access for physicians to assess patient's body condition by combining complementary information provided by multimodality medical images [5]–[7].

A diversity of medical image fusion methods has been proposed in recent decades. Among them, there is a typical type of methods based on the multiscale transform (MST) framework [8]–[17]. Generally, there are three basic steps in an MST based fusion method. Firstly, the source images are decomposed into a series of sub-bands with some strategy. Then, some designed fusion strategies are used to merge transformed coefficients. Finally, the fused image is reconstructed. For instance, Yin *et al.* [18] proposes a medical image fusion method which is based on nonsubsampled shearlet transform (NSST) for decomposition of source images. A parameter-adaptive pulse-coupled neural network (PA-PCNN) model is applied for the fusion of high-frequency bands. Du *et al.* [19] presents a local Laplacian filtering (LLF)-based fusion technique. The source images are transformed with LLF and uses a local energy maximum (LEM) scheme for fusion. Yang *et al.* [20] implements a nonsubsampled contourlet transform (NSCT)-based method. The NCST is performed on preregistered source images to obtain sub-bands with high- and low-frequency. And then the local type-2 fuzzy entropy is introduced for fusion of high-frequency sub-bands and a local energy algorithm is used for low-frequency sub-bandsąŕ fusion. Zhu *et al.* [21] proposes an image fusion approach based on image cartoon-texture decomposition. They first decompose the source images into cartoon and texture components. And

The associate editor coordinating the review of this manuscript and approving it for publication was Huimin Lu.

a spatial-based fusion method is used for cartoon components and a sparse-representation based fusion method is used for texture components.

In these approaches, the interpretability of the sub-bands is weak. In other words, the information included in the sub-bands are hard to explain directly, which leads to the fact that it is difficult to design a fusion strategy. In this paper, to enhance interpretability of the sub-bands and therefore propose a fusion strategy with better results, a medical image fusion method based on spectral total variation (STV) is proposed. The main contributions of our proposed medical image fusion method are outlined as follows:

1) We introduce a STV [22] method into the medical image fusion field. In previous studies, it has been proved that spectral TV helps to extract features in different scale [23]. Therefore, we decide to take advantage of STV to enhance the interpretability of our sub-bands so that we design a new fusion strategy with more effective fusion results.
2) A novel adaptive fusion strategy is presented by decomposing the source images into sub-bands which contain the information of different scale of issues based on spectrum. Because every sub-band contains the issues information of one scale range, the clear meaning of scale information is concluded in sub-bands. Obviously, it enhances the interpretability of sub-images because the sub-images have some visible meanings (the different sizes of the presented issue information). With the clearly visible meanings of the sub-bands, we design a state-of-art image fusion strategy.
3) Experiments have been conducted to analyze the effectiveness of our proposed image fusion method on CT and MR fusion problems. It is demonstrated that our proposed method achieves state-of-art performances on both the subjective and objective evaluation.

The remainder of this paper is organized as follows: In Section II, the technique of STV is briefly introduced. The proposed CT and MR image fusion method via adaptive structure decomposition is presented in Section III. Section IV gives the experimental results and discussion. Finally, Section V concludes the paper.

II. BACKGROUNGS

In this section, we briefly introduce the fundamental theories about the spectral total variation (STV) method.

We aim on decomposing the source images into sub-bands including different scale of issues and organs. And in [22] and [23], it has been proved that spectral TV helps to extract more features in different scale. Motivated by them, we adopt STV to enhance the interpretability of our sub-bands, including clear meaning of scale information, so that we design a new fusion strategy with more effective fusion results. The spectral TV method is based on the total variation (TV) functional, in which the regularizing functional $R(u)$ is defined as

$$R(u) = \int_{\Omega} |\nabla u| dx, \tag{1}$$

where the image domain is defined as Ω, and ∇ means the distributional gradient. The corresponding gradient descent evolution, known as TV flow, is written as

$$\begin{aligned} \frac{\partial u}{\partial t} &= div(\frac{\nabla u}{|\nabla u|}), \quad in(0,\infty)\times\Omega \\ \frac{\partial u}{\partial n} &= 0, \quad on(0,\infty)\times\partial\Omega \\ u(0;x) &= f(x), \quad inx \in \Omega \end{aligned} \tag{2}$$

where $f(x)$ denotes the input image. The scale-space approach is defined as

$$\begin{aligned} u_t(t,x) &= -p(t,x), \\ p(t,x) &\in \partial_u R(u), \end{aligned} \tag{3}$$

where t is defined as time or scale parameter and $u_t(t,x)$ is a set of solutions and $\partial_u R(u)$ is the sub-differential of some regularizing functional. Then, the spectral TV transform is defined by:

$$\gamma(t,x) = u_{tt}(t,x)t. \tag{4}$$

We refer $\gamma(t,x)$ as the spectral component or band at scale t. And u_{tt} is the second derivative of its solution u. Finally, the reconstruction formula is:

$$\zeta(x) = \int_0^{\infty} \gamma(t,x)dt + \overline{f}, \tag{5}$$

where $\overline{f}$ is the mean value of the initial condition. The spectrum $S_f(t)$ is defined as

$$S_f(t) = \|\gamma(t,x)\|_{L^1} = \int_{\Omega} \gamma(t,x)dx. \tag{6}$$

It can be seen as the L_1 amplitude of the response at each scale $t \in [0,\infty]$.

In previous studies, STV has been used for its outstanding effect. In [24], a STV based method is used to obtain saliency map and inject the map into another image. In [23], Zhao *et al.* take advantage of the STV to decompose the source images into many sub-bands, and adopt statistical distribution to construct weight. In comparison, our method has two unique characteristics. Firstly, we obtain our sub-bands in a adaptive way on condition of spectrum, and the sub-bands have strong interpretability so that the meaning including is easy to tell. Secondly, we obtain the local edge energy and the local intensity energy of sub-bands to decide the weight.

III. PROPOSED METHOD

Figure 1 shows the schematic of the proposed CT and MR image fusion via adaptive structure decomposition (ASD). There are three key steps in our method. First, based on the different scales of issues, we self-adaptively decompose source images into corresponding sub-bands with STV technique. In this way, we get the sub-bands with strong interpretability so that we can design an effective fusion method.

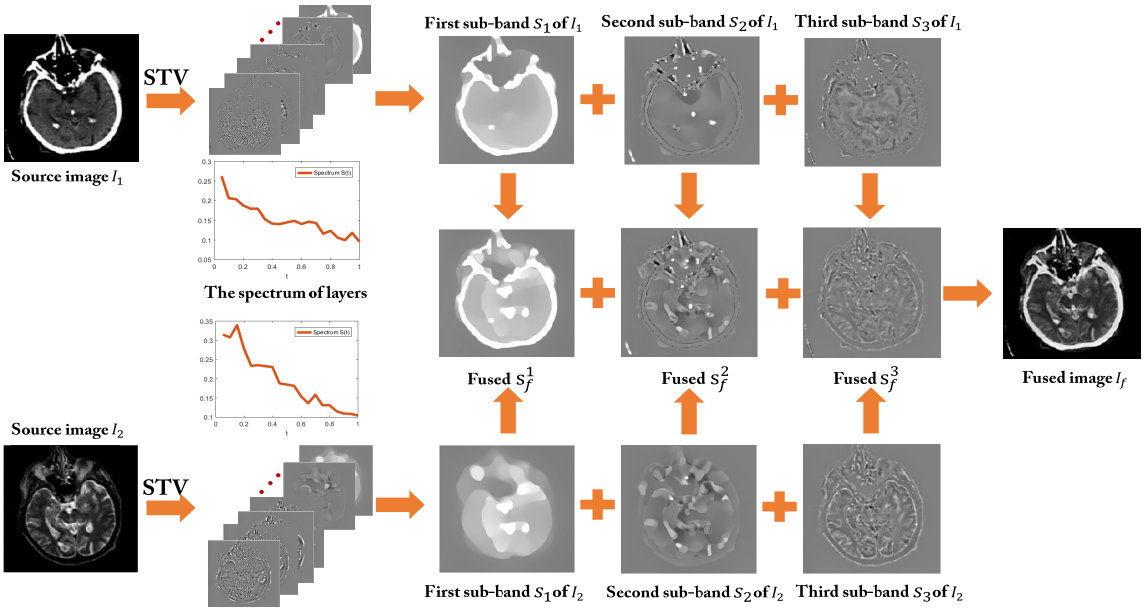

FIGURE 1. Schematic diagram of our proposed image fusion method.

Second, based on the interpretability of sub-bands, for the small scale and middle scale of issues, we extract the edge information from the sub-bands and design the weight of fusion by the local edge energy. And for the large scale of issues, we design the weight of fusion by the local intensity energy. Third, we reconstruct the fused image. Detailed instruction is presented below.

A. ADAPTIVE DECOMPOSITION METHOD

With the support of STV, we obtain N feature layers of different scale issues $\{D^i, i = 1, 2, ..., N\}$ and the rest layer B,

$$\{D^i, B\} = S(I), \tag{7}$$

where $S(I)$ means STV operation for image I. Due to the advantages of STV, each layer presents a different scale of features. However, to get sub-bands which involve a range of scales of issues, we need to divide the $N + 1$ layers into three sub-bands which respectively consist small, middle and large scale of issues.

As we mentioned before, the computed tomography (CT) has an excellent performance on detecting dense structure such as bones and implants and magnetic resonance (MR) provides high-resolution information for soft issues. To enhance the interpretability of sub-bands and therefore design an effective fusion strategy, we decompose the source images according to the different scales of issues. The maxima values of TV spectrum often stand for the main scale feature components (see Figure 2). Therefore, on the basis of maxima values, we manage to design a adaptive decomposition to ensure every sub-band contains one of the two maximum values, which enhance the interpretability of the sub-bands.

To fuse corresponding sub-bands of two source images (I_1 and I_2), we need to decide a uniform dividing rule of sub-bands for two source images. The rest layer of B_{I_1} and B_{I_2} include the large scale of issues so we take them as the first sub-bands s_{I_1} and s_{I_2} (the sub-band with large issues) straightforward.

$$s_{I_1} = B_{I_1}, \tag{8}$$

$$s_{I_2} = B_{I_2}. \tag{9}$$

Due to the dense sampling and tiny features, each feature layer cannot express the overall characteristic clearly. Thus, we decide to divide the N feature layers into 2 sub-bands, which consists of the second sub-band (sub-band with middle scale of issues) and the third sub-band (sub-band with small scale of issues) to express the features of different scales more clearly. Firstly we pick up 2 maximum values of each source image feature layers. As shown in Figure 3, the corresponding layers with the 2 maximum spectrum values are $l^1_{I_1}$, $l^2_{I_1}$, $l^1_{I_2}$ and $l^2_{I_2}$ which are shown as green triangle in Figure 3(b). In Figures 3(c)–(e) are the first, the second, and the third sub-band. Then, to ensure every sub-band include one feature layer with maxima value spectrum, we obtain the boundary of sub-band dividing by:

$$b = \frac{max(l^1_{I_1}, l^1_{I_2}) + min(l^2_{I_1}, l^2_{I_2})}{2}, \tag{10}$$

where b stands for the boundary. Therefore, the second sub-band (the sub-band with middle scale of issues) of I_1 includes $\{D^i, i = 1, 2, ..., b\}$. The third sub-band (the sub-band with small scale of issues) of I_1 includes $\{D^i, i = b + 1, b + 2, ..., N\}$. It is in the same situation for I_2. As shown in Figure 3, the purple point means the boundary of sub-bands. In this way, the sub-bands are divided adaptively.

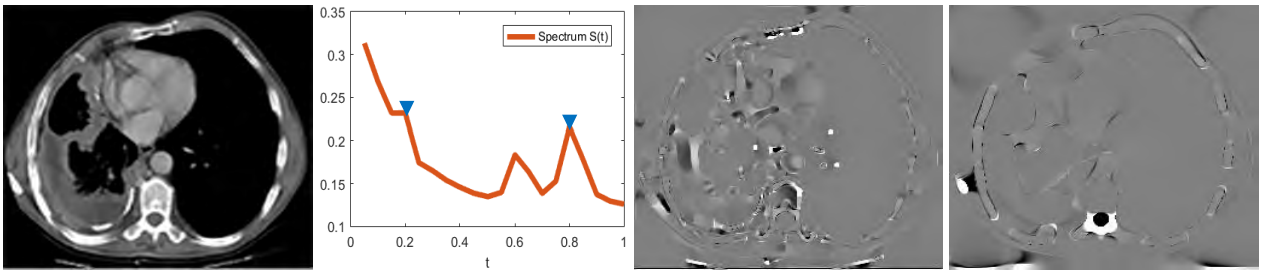

FIGURE 2. An example of the spectrum of main feature layers and the sub-bands divided. (a) Source image. (b) The spectrum of the *N* decomposed layers. (c) The feature layer corresponding to the first maximum value marked by the first blue triangle. (d) The feature layer corresponding to the second maximum value marked by the second blue triangle.

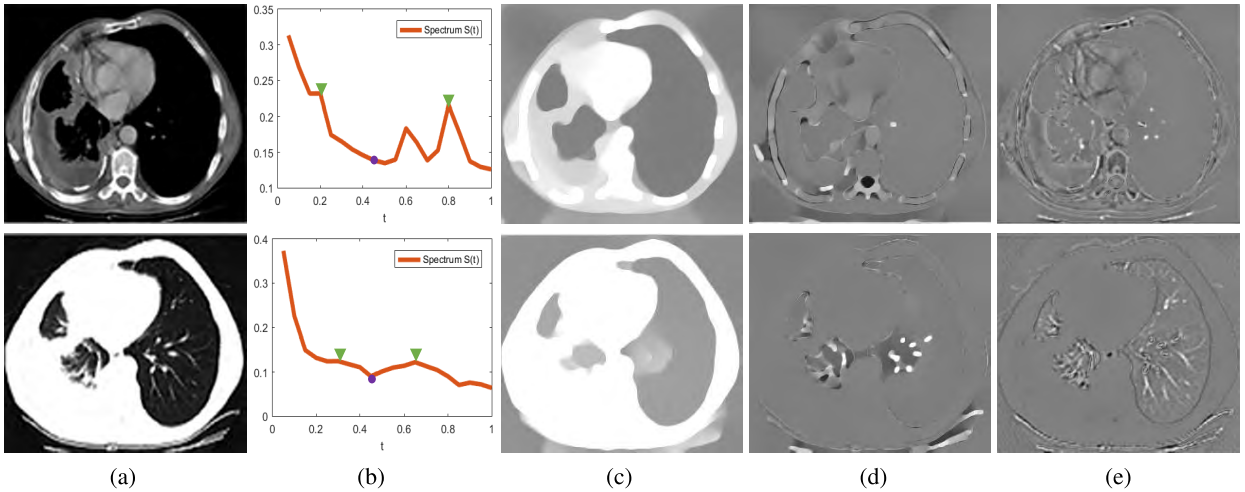

FIGURE 3. An example of a uniform dividing rule for a pair of source images. (a) A pair of source images. (b) The uniform dividing rule (the green triangles mean the maximum values and the purple points mean the boundary). (c)–(e) The first, second, and third sub-band.

Therefore, the second and the third sub-band of image I_1 generated by:

$$s_{I_1}^2 = \frac{1}{b}\sum_{i=1}^{b} D_{I_1}^i, \tag{11}$$

$$s_{I_1}^3 = \frac{1}{N-b-1}\sum_{i=b+1}^{N} D_{I_1}^i. \tag{12}$$

It is the same situation for image I_2.

B. FUSION STRATEGY

The first sub-band (sub-band with large scale of issues) contains the intensity information of issues, so we fuse first sub-bands of two source images with local intensity energy (LIE). We take p_i as the local energy of pixel x_i:

$$p_i = \frac{1}{K}\sum_{i=1}^{K} G_{n*n}(x_i), \tag{13}$$

where $G_{n*n}(\cdot)$ means Gaussian filtering with a window of $n*n$. And the weight of pixel x_i of image I_1 is

$$w_i^1 = \frac{p_i^1}{p_i^1 + p_i^2}. \tag{14}$$

Therefore, the i-th pixel of the fusion result for the first sub-band s_1 is

$$x_i^f = w_i^1 \times x_i^1 + w_i^2 \times x_i^2. \tag{15}$$

There are more details of texture in the second sub-band and the third sub-band because the issues in them are in smaller scales. Therefore, we extract the edge information from the sub-bands and design the weight of fusion by the local edge energy. To consider the edge information of the issues and preserve more details in the second and the third sub-band, we first extract the feature edge. And then we take e_i as the local edge energy (LEE) of pixel x_i:

$$e_i = \frac{1}{K}\sum_{i=1}^{K} G_{n*n}(E(x_i)), \tag{16}$$

where $E(\cdot)$ means the operation of extracting the edges:

$$E(a_{k,s}) = \mid a_{k,s+1} - a_{k,s} \mid + \mid a_{k+1,s} - a_{k,s} \mid, \tag{17}$$

where $a_{k,s}$ stands for the pixel with the location (k, s) in matrix. The weight of pixel x_i of image I_1 is

$$\widehat{w}_i^1 = \frac{e_i^1}{e_i^1 + e_i^2}. \tag{18}$$

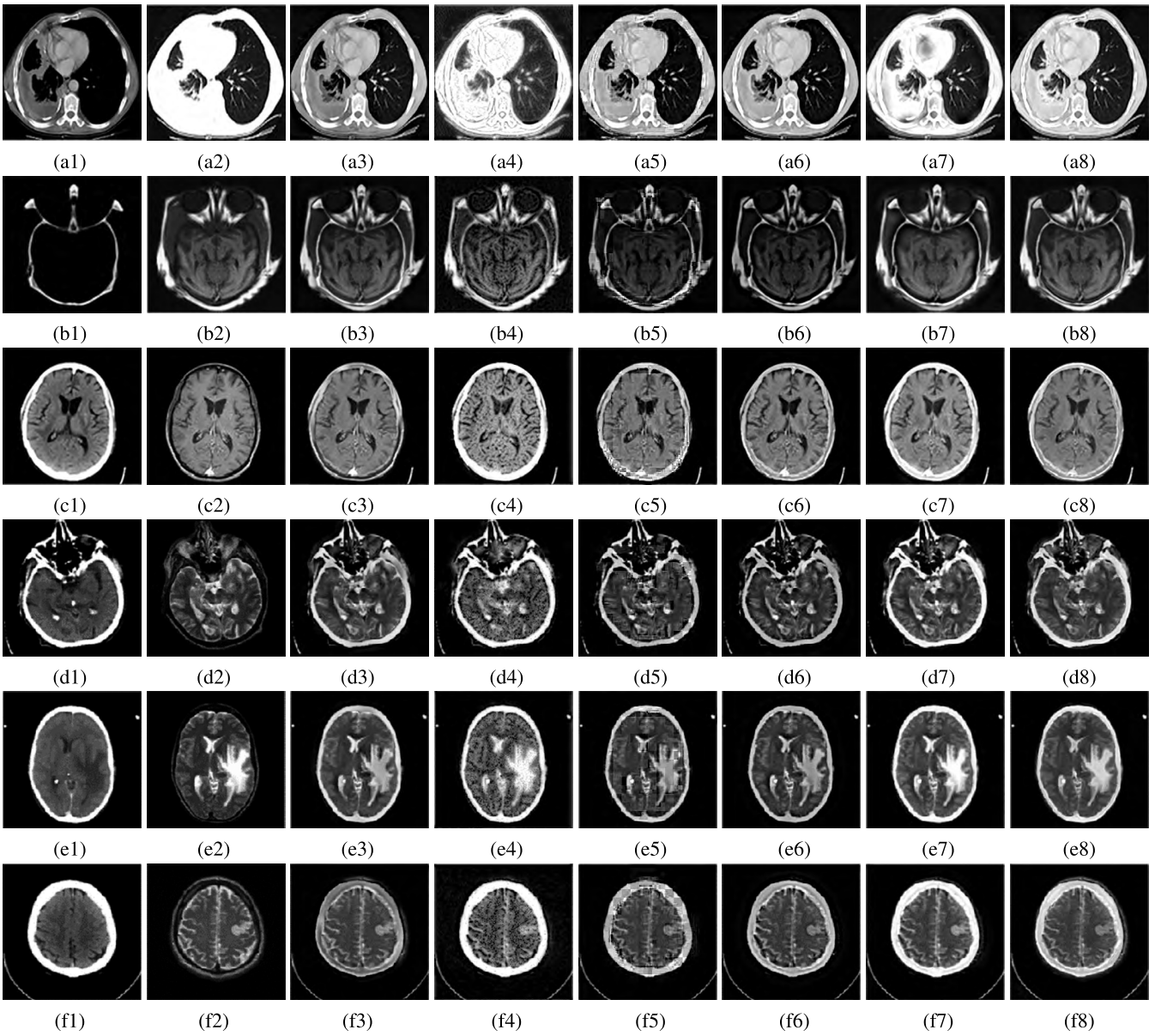

FIGURE 4. Comparison of CT and MR image fusion results. (a1)–(f1) are CT source images; (a2)–(f2) are MR source images; (a3)–(f3) are fusion results of GFF method; (a4)–(f4) are fusion results of LFF method; (a5)–(f5) are fusion results of DWT method; (a6)–(f6) are fusion results of NCST method; (a7)–(f7) are fusion results of NSST method; (a8)–(f8) are fusion results of the proposed method.

And similarly the i-th pixel of the fusion result of the second and the third sub-band s_2 and s_3:

$$x_i^f = \widehat{w}_i^1 \times x_i^1 + \widehat{w}_i^2 \times x_i^2. \tag{19}$$

C. RECONSTRUCTING FUSED IMAGE

Finally, we reconstruct the fused image with

$$I_f = s_f^1 + s_f^2 + s_f^3, \tag{20}$$

where s_f^i means the i-th sub-band of fusion result and I_f stands for the fused image.

IV. EXPERIMENTS

A. EXPERIMENTAL SETTINGS

In this section, we introduce experimental images and algorithm parameter configuration.

1) SOURCE IMAGES

Six pairs of images are used in our experiments to verify the effectiveness of our proposed method. All of these images are collected from the Internet and have been widely used in previous publications related to medical image fusion. The resolution is 256×256 pixels.

2) ALGORITHM PARAMETERS

In our method, the number of feature layers with different scale issues N is taken to 20. And in Eq. (13) and (16), n represents the size of the window of Gaussian filter, which is set $n = 5$, and the variance of the Gaussian filter is taken to 2. The window size for local energy calculation is taken to $K = 25$.

TABLE 1. Quality metrics of different image fusion methods on six image pairs. The best three results are shown in red, blue and green fonts.

No.	Metric	GFF [16]	LFF [19]	DWT [17]	NCST [20]	NSST [18]	Ours
1	EN	7.1351	6.6829	6.7795	6.7539	6.7296	7.3301
	LMI	3.6538	3.2112	3.5368	3.5658	3.3220	4.0938
	QG	0.6890	0.4365	0.5795	0.6617	0.5673	0.6800
2	EN	6.8637	7.0213	6.0718	6.0420	7.0534	6.9415
	LMI	3.4547	2.7189	2.5344	2.4588	2.8067	4.1862
	QG	0.7719	0.5570	0.5954	0.7062	0.7096	0.7645
3	EN	5.1017	5.3188	5.0193	5.5459	5.4588	5.3924
	LMI	3.5317	3.5149	3.5179	3.5266	3.7397	3.7696
	QG	0.6015	0.4389	0.4829	0.5615	0.5469	0.5786
4	EN	5.3671	5.5136	4.9522	5.4198	5.5880	5.6324
	LMI	3.0921	2.8558	2.6845	2.6989	3.2400	3.4289
	QG	0.6270	0.4790	0.5182	0.5785	0.5925	0.5875
5	EN	4.9319	5.2383	4.6807	5.2453	5.1515	5.2948
	LMI	3.5322	3.3360	3.3679	3.3720	3.7719	3.9073
	QG	0.6650	0.4717	0.5912	0.6215	0.6405	0.6430
6	EN	5.0343	6.1343	5.1068	5.3203	5.3977	5.4265
	LMI	3.0657	3.1449	3.0936	3.0259	3.3628	3.7022
	QG	0.5314	0.4654	0.4652	0.5596	0.5537	0.5918
Average	EN	5.7390	5.9848	5.4350	5.7212	5.8965	6.0029
	LMI	3.3893	3.1303	3.1225	3.1080	3.3738	3.8480
	QG	0.6416	0.4746	0.5388	0.6148	0.6017	0.6409

B. COMPARISON WITH STATE-OF-THE-ART METHODS

In this section, we compare our method with other methods on two aspects: qualitative evaluation and quantitative evaluation.

1) QUALITATIVE EVALUATION

Five methods are compared to our proposed fusion method which are the guided filtering fusion (GFF) method [16], the local Laplacian filtering (LLF)-based fusion method [19], the a medical image fusion method which is based on nonsubsampled shearlet transform (NSST) method [18], the nonsubsampled contourlet transform (NSCT) method [20] and the discrete wavelet transform (DWT) method [17]. Experiments are performed mainly on six pairs of images to verify our proposed algorithm. All of these methods are available on the Internet.

Figure 4 shows the result of the experiments on six pairs of CT and MR source images. It can be clearly seen that GFF, DWT and NCST methods lose a large amount of energy. And it leads to the decrease of some important information [see Figures 4(a3)–(f3),(a5)–(f5),(a6)–(f6)]. On the other hand, the LLF method suffers from noise problem [see Figures 4(a4)–(f4)]. In addition, the NSST performs better than them, however, in some regions, detail loss also happens

[see Figures 4(a7)–(f7)]. Our proposed method performs well on both energy preservation and detail extraction.

2) QUANTITATIVE EVALUATION

In order to assess the performances of the fusion results of the methods quantitatively, three widely recognized fusion quality metrics are applied in our experiment, which are entropy (EN), localized mutual information (LMI) [25] and Gradient-Based Index (QG) [26]. For the no-reference images, EN is used as a fusion image metric. And EN can reflects the information included in an image. Therefore, a larger EN metric means an approach with better performance. LMI is a local variation of traditional mutual information (MI) index based on quadtree decomposition. And it can overcome some shortcomings of MI in evaluating fusion performance. In addition, the metric QG is used for the no-reference image fusion quality measure. A higher value of QG indicates a better fusion performance.

Table 1 shows the objective assessment of different methods. In this table, the red data mean the best objective assessment, the blue ones are second best ones and the green ones are the third ones. Our proposed method obviously achieves the best performance in every analyze metric for every pair of images. Especially, for the average metric, our method shows its outstanding and stable performance. Compared to other five fusion methods, our method has obvious advantage on every metric.

V. CONCLUSION

In this paper, an effective CT and MR image fusion method via adaptive structure decomposition is presented. We introduce STV into medical image fusion which can extract features in different scale thereby enhancing the interpretability of the sub-bands. We adaptively decompose the images into three sub-bands: sub-bands with small, middle and large scale of issues. Experiments are performed on representative CT and MR images to validate the effectiveness of our fusion method on both subjective and objective assessment.

REFERENCES

[1] X. Cao, J. Yang, Y. Gao, Q. Wang, and D. Shen, "Region-adaptive deformable registration of CT/MRI pelvic images via learning-based image synthesis," *IEEE Trans. Image Process.*, vol. 27, no. 7, pp. 3500–3512, Jul. 2018.
[2] O. Prakash, C. M. Park, A. Khare, M. Jeon, and J. Gwak, "Multiscale fusion of multimodal medical images using lifting scheme based biorthogonal wavelet transform," *Optik*, vol. 182, pp. 995–1014, Apr. 2019.
[3] H. R. Shahdoosti and Z. Tabatabaei, "MRI and PET/SPECT image fusion at feature level using ant colony based segmentation," *Biomed. Signal Process. Control*, vol. 47, pp. 63–74, Jan. 2018.
[4] S. Singh and R. S. Anand, "Ripplet domain fusion approach for CT and MR medical image information," *Biomed. Signal Process. Control*, vol. 46, pp. 281–292, Sep. 2018.
[5] E. Daniel, "Optimum wavelet-based homomorphic medical image fusion using hybrid genetic–grey wolf optimization algorithm," *IEEE Sensors J.*, vol. 18, no. 16, pp. 6804–6811, Aug. 2018.
[6] W. Zhao and H. Lu, "Medical image fusion and denoising with alternating sequential filter and adaptive fractional order total variation," *IEEE Trans. Instrum. Meas.*, vol. 66, no. 9, pp. 2283–2294, Sep. 2017.
[7] Y. Yang, Y. Que, S. Huang, and P. Lin, "Multiple visual features measurement with gradient domain guided filtering for multisensor image fusion," *IEEE Trans. Instrum. Meas.*, vol. 66, no. 4, pp. 691–703, Apr. 2017.
[8] M. Manchanda and R. Sharma, "An improved multimodal medical image fusion algorithm based on fuzzy transform," *J. Vis. Commun. Image Represent.*, vol. 51, pp. 76–94, Feb. 2018.
[9] H. Li, X. He, D. Tao, Y. Tang, and R. Wang, "Joint medical image fusion, denoising and enhancement via discriminative low-rank sparse dictionaries learning," *Pattern Recognit.*, vol. 79, pp. 130–146, Jul. 2018.
[10] X. Jin, G. Chen, J. Hou, Q. Jiang, D. Zhou, and S. Yao, "Multimodal sensor medical image fusion based on nonsubsampled shearlet transform and S-PCNNs in HSV space," *Signal Process.*, vol. 153, pp. 379–395, Dec. 2018.
[11] P. Chai, X. Luo, and Z. Zhang, "Image fusion using quaternion wavelet transform and multiple features," *IEEE Access*, vol. 5, pp. 6724–6734, 2017.
[12] H. M. El-Hoseny, W. A. EI-Rahman, E. M. El-Rabaie, F. E. A. EI-Samie, and O. S. Faragallah, "An efficient DT-CWT medical image fusion system based on modified central force optimization and histogram matching," *Infr. Phys. Technol.*, vol. 94, pp. 223–231, Nov. 2018.
[13] J. Du, W. Li, B. Xiao, and Q. Nawaz, "Union Laplacian pyramid with multiple features for medical image fusion," *Neurocomputing*, vol. 194, pp. 326–339, Jun. 2016.
[14] X. Liu, W. Mei, and H. Du, "Multi-modality medical image fusion based on image decomposition framework and nonsubsampled shearlet transform," *Biomed. Signal Process. Control*, vol. 40, pp. 343–350, Feb. 2018.
[15] B. Yang and S. Li, "Multifocus image fusion and restoration with sparse representation," *IEEE Trans. Instrum. Meas.*, vol. 59, no. 4, pp. 884–892, Apr. 2010.
[16] S. Li, X. Kang, and J. Hu, "Image fusion with guided filtering," *IEEE Trans. Image Process.*, vol. 22, no. 7, pp. 2864–2875, Jul. 2013.
[17] *Image Fusion Toolbox for MATLAB 5.X*. Accessed: Oct. 2016. [Online]. Available: http://www.metapix.de/toolbox.htm/
[18] M. Yin, X. Liu, Y. Liu, and X. Chen, "Medical image fusion with parameter-adaptive pulse coupled neural network in nonsubsampled shearlet transform domain," *IEEE Trans. Instrum. Meas.*, vol. 68, no. 1, pp. 49–64, Jan. 2019.
[19] J. Du, W. Li, and B. Xiao, "Anatomical-functional image fusion by information of interest in local Laplacian filtering domain," *IEEE Trans. Image Process.*, vol. 26, no. 12, pp. 5855–5866, Dec. 2017.
[20] Y. Yang, Q. Yue, S. Huang, and P. Lin, "Multimodal sensor medical image fusion based on type-2 fuzzy logic in NSCT domain," *IEEE Sensors J.*, vol. 16, no. 10, pp. 3735–3745, May 2016.
[21] Z. Zhu, H. Yin, Y. Chai, Y. Li, and G. Qi, "A novel multi-modality image fusion method based on image decomposition and sparse representation," *Inf. Sci.*, vol. 432, pp. 516–529, Mar. 2018.
[22] G. Gilboa, "A total variation spectral framework for scale and texture analysis," *SIAM J. Imag. Sci.*, vol. 7, no. 4, pp. 1937–1961, 2014.
[23] W. Zhao, H. Lu, and D. Wang, "Multisensor image fusion and enhancement in spectral total variation domain," *IEEE Trans. Multimedia*, vol. 20, no. 4, pp. 866–879, Apr. 2018.
[24] E. Hait and G. Gilboa, "Spectral total-variation local scale signatures for image manipulation and fusion," *IEEE Trans. Image Process.*, vol. 28, no. 2, pp. 880–895, Feb. 2019.
[25] M. Hossny, S. Nahavandi, D. Creighton, and A. Bhatti, "Image fusion performance metric based on mutual information and entropy driven quadtree decomposition," *Electron. Lett.*, vol. 46, no. 18, pp. 1266–1268, 2010.
[26] C. S. Xydeas and V. Petrovic, "Objective image fusion performance measure," *Electron. Lett.*, vol. 36, no. 4, pp. 308–309, Feb. 2000.

FAN ZHAO received the B.S. degree from the Changchun University of Science and Technology, Changchun, China, in 2011, and the M.S. and Ph.D. degrees from the Changchun Institute of Optics, Fine Mechanics and Physics, Chinese Academy of Sciences, Changchun, in 2017. She is currently a Faculty Member with the Dalian Institute of Chemical Physics, Chinese Academy of Sciences. Her research interests include object recognition and low-level vision tasks.

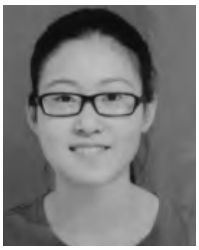

GUIYING XU is currently pursuing the B.S. degree with the Dalian University of Technology (DUT), Dalian, China. Her current research interest includes low-level vision tasks.

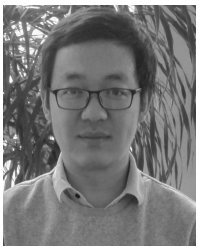

WENDA ZHAO received the B.S. degree from Jilin University, Changchun, China, in 2011, and the M.S. and Ph.D. degrees from the Changchun Institute of Optics, Fine Mechanics and Physics, Chinese Academy of Sciences, Changchun, in 2016. He is currently a Faculty Member with the School of Information and Communication Engineering, Dalian University of Technology (DUT). His research interests include deep learning and computer vision.